

The Langmuir Probe and Waves (LPW) Instrument for MAVEN

L. Andersson¹  · R.E. Ergun^{1,2} · G.T. Delory³ ·
A. Eriksson⁴ · J. Westfall¹ · H. Reed¹ · J. McCauly³ ·
D. Summers¹ · D. Meyers¹

Received: 17 July 2014 / Accepted: 14 July 2015 / Published online: 17 September 2015
© Springer Science+Business Media Dordrecht 2015

Abstract We describe the sensors, the sensor biasing and control, the signal-processing unit, and the operation of the Langmuir Probe and Waves (LPW) instrument on the Mars Atmosphere and Volatile EvolutioN (MAVEN) mission. The LPW instrument is designed to measure the electron density and temperature in the ionosphere of Mars and to measure spectral power density of waves (DC–2 MHz) in Mars’ ionosphere, including one component of the electric field. Low-frequency plasma waves can heat ions resulting in atmospheric loss. Higher-frequency waves are used to calibrate the density measurement and to study strong plasma processes. The LPW is part of the Particle and Fields (PF) suite on the MAVEN spacecraft. The LPW instrument utilizes two, 40 cm long by 0.635 cm diameter cylindrical sensors with preamplifiers, which can be configured to measure either plasma currents or plasma waves. The sensors are mounted on a pair of ~ 7 meter long stacer booms. The sensors and nearby surfaces are controlled by a Boom Electronics Board (BEB). The Digital Fields Board (DFB) conditions the analog signals, converts the analog signals to digital, processes the digital signals including spectral analysis, and packetizes the data for transmission. The BEB and DFB are located inside of the Particle and Fields Digital Processing Unit (PFDPU).

Keywords Mars · Langmuir Probe · Waves instrument · Ionosphere · Electron temperature

1 Introduction

The LPW instrument is designed to measure the electron density (n_e) and temperature (T_e) in the ionosphere of Mars and detect waves that can heat ions, resulting in atmospheric

✉ L. Andersson
laila.andersson@lasp.colorado.edu

¹ LASP, University of Colorado, Boulder, CO, USA

² APS, University of Colorado, Boulder, CO, USA

³ SSL, University of California, Berkeley, CA, USA

⁴ Swedish Institute for Space Physics, Uppsala, Sweden

loss. Electron density and temperature influences photochemical reaction rates that regulate atmospheric loss so measurement of n_e and T_e is critical to MAVEN's science goals. Much of our present day understanding and modeling of Mars' ionosphere is based primarily on two altitude profiles from the Viking Landers (Hanson et al. 1977). In particular, these data contain the best-known electron temperature profiles. Density profiles of Mars' ionosphere have been measured by the MARSIS instrument on the MEX satellite (e.g. Gurnett et al. 2005; 2008). The MARSIS instrument uses sounding to derive the local plasma density and n_e profiles. The Phobos mission included an electric field measurement (Grard et al. 1989; Nairn et al. 1991) providing wave spectral power density, but was not focused on Mars' upper atmosphere. The LPW is designed to measure n_e and T_e profiles of Mars' ionosphere over a broad range of latitude, solar azimuth angle, and magnetic field conditions. The LPW also measures one direction of the electric field waves to determine if ion heating through wave-particle interaction can be an important mechanism of atmospheric loss at Mars.

1.1 Measurement Objectives

Previous missions have established that the most important range of n_e in Mars' ionosphere is from $\sim 200 \text{ cm}^{-3}$ to $\sim 2 \times 10^5 \text{ cm}^{-3}$ (e.g. Gurnett et al. 2008). The LPW instrument is optimized to measure n_e in a range covering $\sim 100 \text{ cm}^{-3}$ to 10^6 cm^{-3} . The impact of electrons on photochemical reactions is not significant if electron densities are lower than $\sim 100 \text{ cm}^{-3}$. T_e measurements of Mars' ionosphere are sparse, so the LPW is optimized to measure T_e in the broad range of 500–50000 K. The scientific goals of MAVEN call for an absolute accuracy of $\sim 20 \%$ and a relative accuracy of $\sim 5 \%$ of n_e profiles from the density peak of the dayside ionosphere (typically at 150 km in altitude with n_e on the order of 10^5 cm^{-3}) to the nominal ionopause ($\sim 400 \text{ km}$ in altitude with $n_e \sim 2 \times 10^2 \text{ cm}^{-3}$). Night side densities are expected to be significantly lower. The Langmuir Probe (LP) technique (Mott-Smith and Langmuir 1926) is used for the primary measurement of n_e and T_e .

The required time resolution or cadence of the n_e and T_e measurements is derived from the needed spatial resolution in altitude. The scale height of the Mars' ionosphere can be as small as $\sim 10 \text{ km}$, so the goal is to have better than $\sim 2 \text{ km}$ altitude resolution for the global data set. The vertical component of the spacecraft velocity is significantly less than 500 m/s at altitudes below 400 km, so a 4 second time resolution is more than adequate to achieve 2 km resolution in altitude. The spacecraft velocity is primarily parallel to Mars' surface at the lowest altitude and the horizontal resolution at 4 s cadence with an expected velocity of 4.3 km/s is $\sim 17 \text{ km}$.

Observations of plasma waves, electron fluxes, and ion fluxes in Mars' ionosphere (Lundin et al. 2004; Espley et al. 2004; Brain et al. 1973) indicate that ion heating or acceleration by electric fields may have had a significant impact on Mars' atmospheric loss (Ergun et al. 2006). Waves or fluctuations near the ion gyrofrequencies (0.05 Hz–10 Hz) are particularly efficient at ion acceleration. Higher frequency waves may indicate electron acceleration or auroral-like processes.

To measure waves near the ion gyrofrequency and above, the LPW instrument has included one component of electric field wave power at frequencies between 0.05 Hz and 10 Hz with an instrument sensitivity of $10^{-8} (\text{V/m})^2/\text{Hz} (f_o/f)^2$ with $f_o = 10 \text{ Hz}$ and at 100 % bandwidth. Electric fields at higher-frequency, up to $\sim 2 \text{ MHz}$ are measured to calibrate the LP and to study strong plasma processes.

1.2 Measurement Techniques

1.2.1 Langmuir Probe

The electron density and temperature are derived from the current-voltage (I - V) characteristic, a well-established technique (Mott-Smith and Langmuir 1926; Allen 1992; Brace 1998; Gurnett et al. 2004; Eriksson et al. 2007). With this technique, the current from the plasma to a voltage-biased probe is measured over a range of probe voltages, creating an I - V characteristic. I - V characteristics are fit to determine the n_e , T_e , ion density (n_i), the spacecraft potential (V_{SC}), and properties of photoelectrons. The “LP sweep” contains 128 programmable voltages inside of a range from -50 V to 50 V. The minimum step size is ~ 24 mV. The sweeps are performed in one second (configurable) and are pseudo-logarithmic, designed to have the smallest voltage steps near zero potential to optimize the accuracy of the T_e measurement. The dwell time at each step is 7.8 ms in the nominal configuration for Mars’ ionosphere. An examples of an LP sweep is shown in Sect. 6.

To cover the large range of n_e and T_e , the LPW sensors detect a wide range of probe current (I_p), from -0.02 mA to 0.2 mA at ~ 0.8 nA resolution. Here, positive current is electron collection. The resolution is limited by the analog-to-digital conversion (16 bit at $1/4$ bit accuracy, averaged to 20 bits).

This measurement technique, when implemented on a spacecraft, requires several other factors to be taken into consideration. Two sensors are used for the LP sweep since one of the probes could be in the spacecraft wake. The ratio of conductive surface area of the sensors to that of the spacecraft needs to be such that V_{SC} does not significantly change during a sweep. The net current to the entire spacecraft (including the LP sensor) must be zero. When biased at a positive voltage, the LP sensor attracts electrons, so the rest of the spacecraft must attract an ion current or emit photoelectrons. Since the ion thermal velocities are considerably lower than that of electrons, the spacecraft (minus the LP sensor) must have a significantly larger collection area compared to the LP sensor area. On MAVEN, the area ratio of the spacecraft (minus the LP sensor) to LP surface varies between ~ 80 to ~ 500 depending on the spacecraft orientation with respect to the plasma flow. The large variations in effective surface area reflect the differences in conduction between the surfaces on the spacecraft. For example, the solar arrays are non-conductive and the high-gain antenna cover is resistive. The LPW has an additional feature such that, during an LP sweep, as one probe performs the sweep the other probe monitors the plasma potential so that a change in V_{SC} can be detected.

V_{SC} is influenced by plasma conditions, spacecraft attitude and velocity, and sunlight so it may vary dramatically during an orbit. The LP sweep is automatically adjusted to account for V_{SC} . The “sweep offset” is adjusted to a voltage level at which the absolute value of the current was near a minimum in the previous sweeps. A discussion of the automatic offset adjustment is in Sect. 3. The LPW can operate well if -45 V $< V_{SC} < 45$ V.

Photoelectron currents can interfere with the fitting process that determines n_e and T_e , particularly in low-density (< 1000 cm $^{-3}$) plasmas. These currents come in two forms: photoelectron currents from the spacecraft to the probe and photoelectron currents emitted by the probe. The photoelectron currents from the spacecraft to the probe are minimized by a combination of long booms (7.1 m) and biased surfaces near the sensors (guards and stubs). The photoelectron currents emitted by the probe to the plasma (or spacecraft) must be removed in data analysis. Surface treatments of the probe are designed to have a well-known and constant photoelectron current so that the removal of the photoelectron currents does not cause significant errors.

1.2.2 Electric Fields, Waves, and Sounding

One component of the electric field is measured using the double-probe technique (e.g., Fahleson 1967) from DC to ~ 2 MHz. The electric field measurement uses the same sensors as the LPW with different preamplifiers that are connected and disconnected via a relay. The low-frequency electric field measurement includes piecewise continuous waveforms of one component of the electric field with a range of ± 1 V/m and a resolution 0.3 mV/m. The data processing also includes LF spectra (1 Hz to ~ 500 Hz), MF spectra (~ 100 Hz to ~ 32 kHz), and HF spectra (~ 10 kHz to ~ 2 MHz). The LPW includes burst waveform capture in all three bands.

The absolute accuracy of the n_e measurement can be greatly improved (to $< 5\%$) if the frequency of Langmuir waves or upper hybrid waves can be determined (see Sect. 3.2.5). The LPW includes an electric field wave receiver that covers the frequency range up to 2 MHz. The upper hybrid or plasma frequencies within this range correspond to densities between ~ 10 cm $^{-3}$ and 5×10^4 cm $^{-3}$. The receiver can be sensitive to plasma waves with a spectral power density as low as 3×10^{-14} (V/m) 2 /Hz at 1 MHz. The electrostatic cleanliness program on the MAVEN spacecraft did not include conductive solar arrays, as the process was deemed too expensive, so spacecraft noise is expected to dominate the noise floor of the plasma wave receiver. The noise floor is to be determined once MAVEN is in orbit around Mars. When measuring natural emissions, these data are called “passive spectra”.

Since naturally occurring Langmuir or upper hybrid waves may not be detected regularly, the MAVEN LPW can stimulate the surrounding plasma with a 5 V pseudo-random sequence using the stacer booms as transmitting elements. This relaxation sounding technique (e.g. Etcheto et al. 1981) measures the plasma frequency in quiet environments. The sequence is to broadcast using both antennas as a dipole, receive the plasma wave electric field immediately after the broadcast is turned off, and record the spectra. These data are called “active spectra”.

1.3 Instrument Overview

Figure 1 displays a block diagram of the LPW instrument. The location of the sensors on the spacecraft is depicted in Fig. 2. The instrument includes two, 7.1 m stacer booms (Pankow et al. 2001; Bale et al. 2008), which support preamplifiers and 40 cm by 0.635 cm sensors. The 7.1 m stacer booms are to be deployed once in orbit at Mars. The sensors are titanium rods with a titanium nitride surface (Eriksson et al. 2007). The preamplifiers between the sensors and the stacer boom can operate in one of two modes. In LP mode, the sensor is biased at a programmed set of potentials (with respect to the spacecraft) while the LP preamplifier measures the currents. In waves or voltage mode (marked “V” in Fig. 1), the sensor has a small current bias optimized so that the sensor floats near the plasma potential. The waves preamplifier measures the sensor potential. The potential of the surfaces near to the sensor, called guards and stubs, are controlled.

The Boom Electronics Board (BEB) provides floating power to the preamplifiers, bias voltages and currents to the preamplifiers, and bias voltages for the guards and stubs. The floating power allows the preamplifiers to operate between -90 V and 90 V from the spacecraft potential, which can dramatically differ from the plasma potential. The BEB also produces the signals to the relay, which switches between the LP preamplifier and waves preamplifier.

The Digital Fields Board (DFB) has analog filters and analog switches that feed two analog-to-digital (A/D) converters. One A/D converter runs at ~ 4.2 Msamples/s (2^{22} samples/s) with 14 bit resolution. It is dedicated to the high-frequency electric field waves signal.

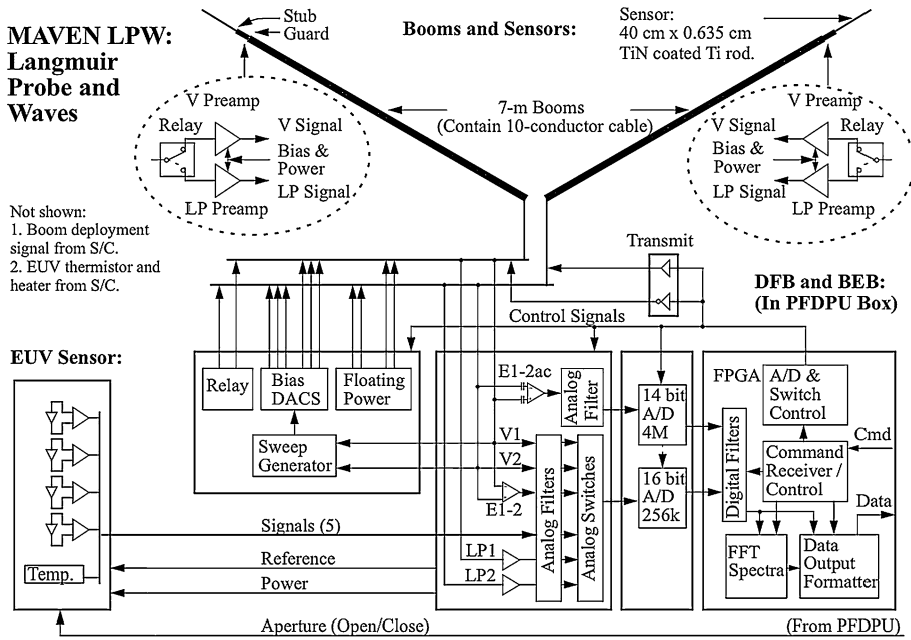
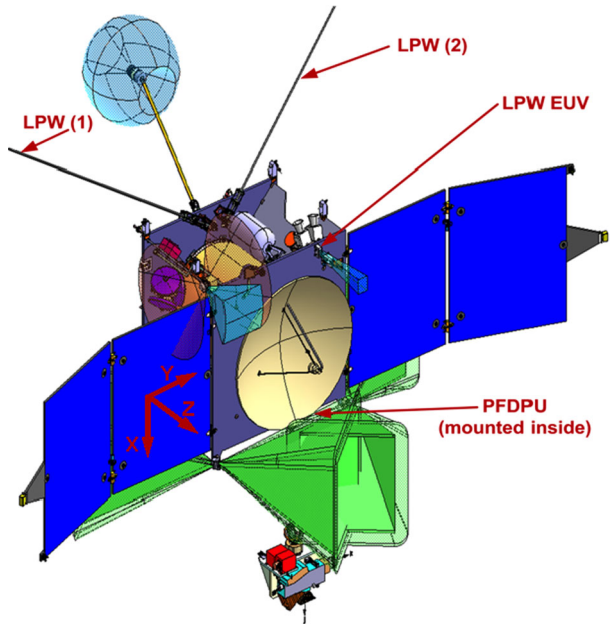


Fig. 1 A block diagram of the MAVEN LPW instrument

Fig. 2 The location of the sensors associated with the LPW. The field-of-view of all of the PF instruments on the spacecraft body are included in the illustration (EUV, SWEA, SWIA, and SEP). The full length of the LPW booms is not shown



The second A/D converter runs at ~ 262 ksamples/s (2^{18} samples/s) at 16-bit precision. It converts all other signals including the LP signals, the LF and MF waves signals, and those from the EUV.

The DFB contains an ACTEL RTAX2000 field-programmable gate array, which carries out all of the digital signal processing, including Fast Fourier Transforms (FFT), digital filtering, burst memory, data compression, and data packetizing. Other tasks include LP sweep control, surface bias control, relay control, and transmission for active spectra.

The LPW instrument is a part of the Particle and Fields (PF) suite. The suite contains the following instruments: Suprathermal and Thermal Ion Composition (STATIC) (McFadden et al. 2014, [this issue](#)), Solar Wind Electron Analyzer (SWEA) (Mitchell et al. 2014, [this issue](#)), Solar Wind Ion Analyzer (SWIA) (Halekas et al. 2015), Solar Energetic Particle SEP (Larson et al. 2014, [this issue](#)), and Magnetometer (MAG) (Connerney et al. 2015). The PF suite is designed to provide a complete set of plasma instruments to study the plasma at Mars in order to understand the atmospheric loss.

The PF suite is controlled by the Particle and Fields Data Processing Unit (PFDPU). The BEB and the DFB boards are physically located inside of the PFDPU box. Since PFDPU and BEB/DFB are built at different institutions, the BEB/DFB are designed to operate as autonomously as possible. The key functions of the PFDPU for the LPW are to control the power-on and power-off sequences, pass to the LPW its commands, control the EUV aperture, and receive the LPW data packets and redirect them to either the archive memory inside the PFDPU or the spacecraft memory for later downlink. Data from the PFDPU archive memory must be requested for transmission.

The spacecraft operates the one-time mechanical release mechanisms and the heaters associated with the LPW and EUV. Mechanical release mechanisms include the stacer deployment and the EUV cover. Spacecraft controlled heaters are located on the boom deployment units and the EUV sensor box.

One part of the instrument, the Extreme UltraViolet sensor, is described in a companion paper (Epavier et al. 2014, [this issue](#)). The EUV signals are received and processed by the LPW so the EUV signal processing is included in this article.

1.4 Operations Overview

The LPW performs both LP sweeps and wave measurements by cycling through the measurements. An individual sensor cannot operate in LP mode and waves mode simultaneously. A master cycle (Fig. 3) is defined to contain four sub-cycles, which perform a specific measurement. Each of the four sub-cycles has the same time duration, which is 1/4 of the master cycle. The master cycle length can be configured from 4 s (1 s long sub-cycles) to 256 s (64 s long sub-cycles).

The planned master cycle is outlined in Fig. 3. The LPW instrument begins by performing a 128-point sweep on sensor 1 while operating as a LP, labeled Sweep 1 in Fig. 3, while recording the DC potential on sensor 2 (configured in voltage mode). Next, both sensors are set to waves mode and passive wave spectra are acquired. The LPW then performs a sweep on sensor 2 (configured as a LP) while recording the DC potential on sensor 1. The last sub-cycle executes the relaxation sounder (active spectra). A white-noise transmission is made on the stacers and the wave spectra are recorded.

Since the science focus of the LPW instrument is at low-altitudes ($< \sim 500$ km) and during deep dips, the master cycle length at low altitudes is configured to 4 s, the fastest operation (Fig. 4). Between ~ 500 km and ~ 2000 km there are several important plasma boundaries. The plasma density is lower, so the master cycle is planned to be set at 8 s, allowing for 2 s sweeps with longer (~ 15 ms) dwell times at each voltage step. At higher altitudes, the master cycle is set to 64 s, primarily for solar wind monitoring. Data limitations play an important role in the LPW operations. Roughly 60 % of the data allocation is used below ~ 500 km, which comprises only ~ 8 % of the orbit.

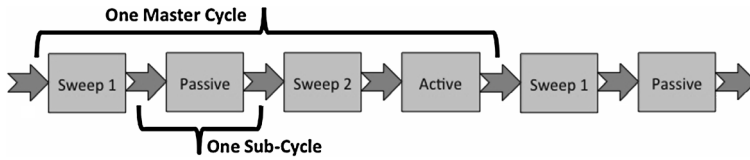
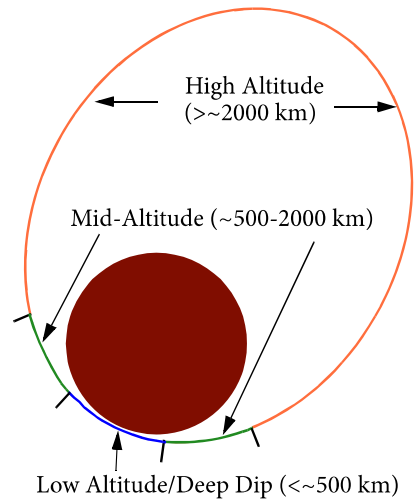


Fig. 3 The planned master cycle. The LPW cycles through LP mode and W (or wave mode) to measure n_e , T_e , and plasma waves

Fig. 4 The LPW basic configuration is to operate with a 4 s master cycle at the lowest altitudes ($< \sim 500$ km), an 8 s master cycle at mid-altitudes (~ 500 km to ~ 2000 km), and a 64 s master cycle at high altitudes



The LPW instrument is highly configurable so that it can operate in a variety of plasma conditions and can focus on specific scientific phenomenon. Equally as important, the LPW instrument can be fine-tuned after orbital insertion to enhance scientific return. The initial configurations, discussed in this article, are based on predicted conditions along the MAVEN orbit. The LPW sweep tables, sensor biasing (including waves bias current), and biasing tables for the guards and stubs are automatically changed based on the predicted orbital position to optimize the measurements. For example, the sweep tables have a narrow voltage range at low altitudes where dense plasma is expected (-5 V to 5 V; see discussion on automatic offset adjustment). The voltage range is expanded when in the solar wind to -45 V to 45 V. The instrument also has a specific configuration designed for when the spacecraft is in Mars' umbra.

2 Sensors, Preamplifiers, and Booms

2.1 Stacer Booms

Two booms and sensors are used for the LP and waves measurements. The booms are rotated in the $-X$ direction 30° from the Z - Y plane of the spacecraft. In Fig. 2, Z is the direction normal to the solar arrays, Y is the direction along the length of the solar arrays, and X is along the width of the solar arrays. They are also rotated 18° from the x - y plane in the $-z$ direction. The boom orientations are designed (1) to avoid the spacecraft wake,

(2) to maximize sensor separation, (3) to distance the sensors from the solar arrays, (4) to remain clear of thruster plumes, and (5) to avoid impinging on the fields of view of other instruments. The booms are 110.9° from each other. The separation between the sensors, center-to-center, is 12.68 m.

The two LPW booms are nearly identical. A diagram of one boom is shown in Fig. 5. Each boom unit has a ~ 7.1 m long stacer held to the spacecraft by a deployment assist device (DAD). On the spacecraft end of a stacer is a flyweight braking mechanism, which reels out a ten-conductor cable that carries signals between the BEB and the preamplifiers and also serves to mechanically control the deployment rate and constrain the stacer length once deployed. At the outer end of each of the stacer booms are a preamplifier and a sensor, which are described later. These stacer booms, DAD systems, and flywheel braking mechanisms have been described in several articles (Pankow et al. 2001; Bale et al. 2008; Bonnell et al. 2008), so our description is brief.

A stacer is a rolled, flat strip of BeCu with a constant helical pitch. The helical pitch creates a ~ 10 N axial push force once the stacer is rolled into a short cylinder. The strip pitch, thickness, width, and diameter are optimized for a particular application. The BeCu stacer is stowed for launch in a coiled state inside a housing and DAD. A primary advantage of the stacer boom is its thermal symmetry once deployed. The helical wrap allows for circumferential heat flow. In spite of the relatively good thermal properties, the stacer booms, when in sunlight, are expected to arc away from the sun by ~ 14.5 cm ($\sim 1.2^\circ$) since the MAVEN spacecraft is 3-axis stabilized. These values are derived from thermal modeling. At terminator crossings, the arcing develops over several minute time periods and does not disturb the measurements from the LPW or other instrument measurements.

The DAD is spring-loaded and serves to initiate the stacer deploy after its release by a Frangibolt actuator controlled by the spacecraft. After the DAD is fully deployed, the stacer continues to deploy through two sets of roller nozzles, which ultimately provide lateral stability of the main stacer when fully deployed. The stacer deploys using its own strain energy. Once fully deployed, the stacer is ~ 7.1 m in length. The spacecraft end of the stacer has a diameter of ~ 33 mm while the preamplifier end is ~ 18 mm.

On the MAVEN mission, the stacer is electrically isolated from the DAD, its housing, and the spacecraft. The stacers are electrically controlled by the DFB. They are grounded by the DFB in nominal use and are used as broadcasting antennas for relaxation sounding.

2.2 Preamplifiers and Sensors

Each of the sensor and preamplifier units must act as a Langmuir probe and make wave measurements. To make both measurements, each of the booms has a single sensor that can input to one of two preamplifiers, an LP preamplifier and a waves preamplifier. The selection is controlled by a relay (Fig. 1). The LP preamplifier measures the current to the sensor, which is maintained at a programmable potential. The waves preamplifier measures the potential of the sensor. The waves preamplifier system can add a bias current to the sensor.

2.2.1 Preamplifier and Sensor Requirements

The critical aspect of the LP operation is to collect electron or ion currents to determine plasma properties. Since photoelectron currents, those collected by the sensor from surrounding surfaces (I_{phc}) and those emitted by the sensor (I_{phe}), must be removed from the measurement, they need to be well controlled. The sheath resistance between the sensor and

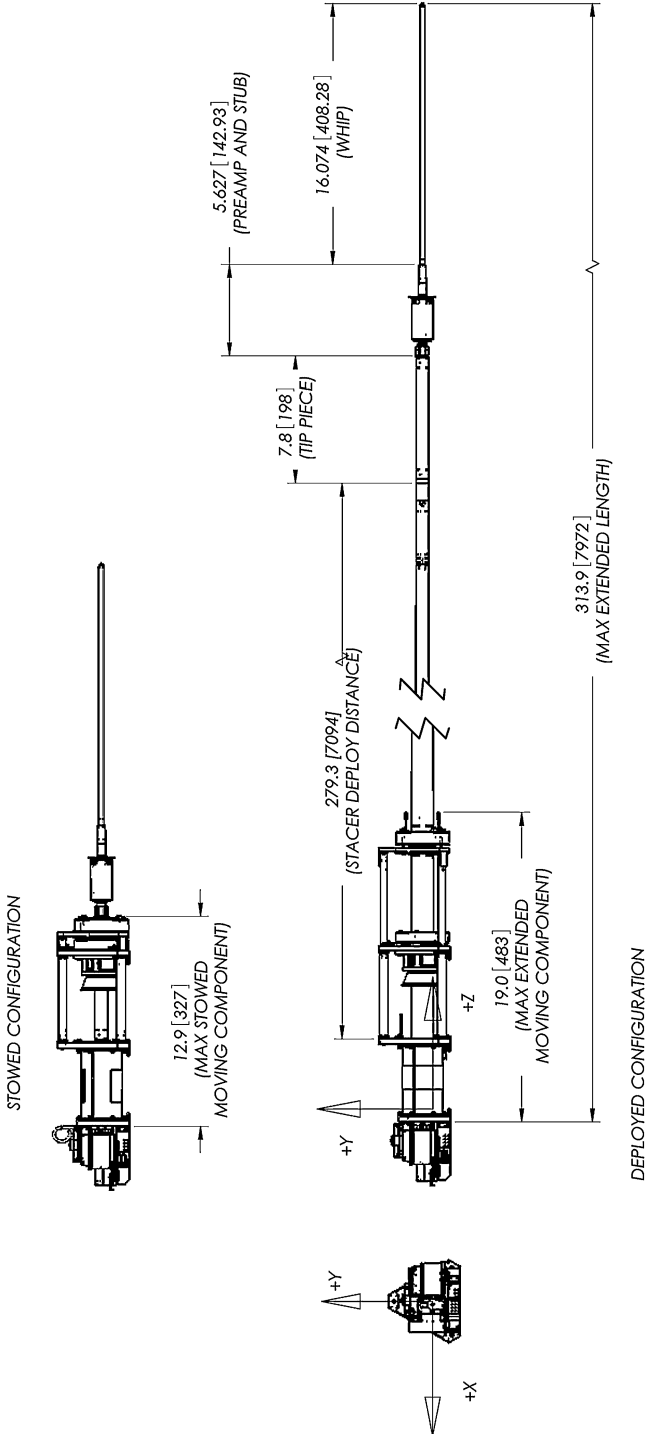
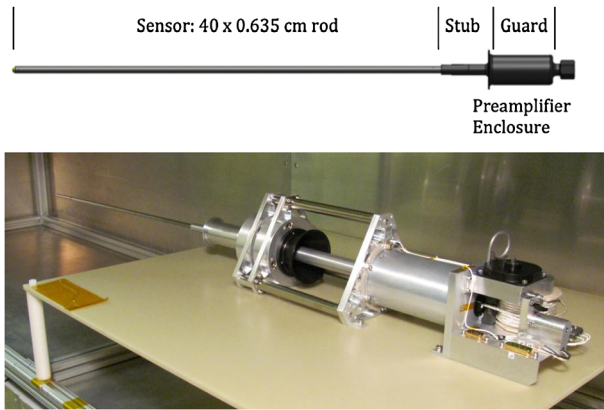


Fig. 5 Diagram of the boom and sensor system in stowed and deployed configuration. Here, the “whip” refers to the sensor. The tip piece is electrically connected to the boom and has the same conductive surface

Fig. 6 *Top*, the mechanical design of the sensor and preamp. *Bottom*, the LPW boom and sensor in a test chamber



surrounding plasma can be tens of kOhms to tens of MOhms. The sensor must be resistively isolated from the spacecraft and have a high-impedance preamplifier $>10^{11}$ Ohms.

The sensor area is a key design consideration. The area must be large enough to yield measurable electron and ion currents. However, the sensor area must be small compared to the spacecraft area so that V_{SC} is stable over a sweep. Another design constraint is the sensor size compared to the plasma sheath size. A small sensor (compared to the Debye length) operates in an orbit-limited regime whereas a large sensor operates in a sheath-limited regime.

In measuring plasma waves, capacitive coupling of the sensor to the plasma is dominant above ~ 100 Hz (dramatically varies with plasma conditions, e.g. Bale et al. 2008). The free-space capacitance or “sheath” for a cylinder is estimated at (Jackson 1975):

$$C_{Sh} \approx \frac{2\pi\epsilon_0}{\ln(L/r)} \left[1 + \frac{(1 - \ln(2))}{\ln(L/r)} \right]$$

where L and r are the sensor length and radius, which result in ~ 10 pF capacitance for the MAVEN sensors. The stray capacitance from the sensor to any part of the spacecraft must be minimized so that the wave signal is not attenuated.

2.2.2 Sensor Design

The LPW sensors are diagramed in Fig. 6. The sensor is a 40 cm by 0.635 cm titanium tube with a TiN surface, which acts as the physical collection area (~ 80 cm²). This area is roughly 100 times smaller than the expected collection area of the spacecraft. The sensor is electrically connected to the inputs of the preamplifiers. The collection area results in ~ 20 nA thermal electron currents at the lowest densities ($\sim 10^2$ cm⁻³) and ~ 0.2 mA if the n_e were to reach 10^6 cm⁻³.

The cylindrical sensor has the advantage that the current collection properties (e.g., focus factor) are well behaved and well understood analytically even with small Debye lengths (Chen 1965; Brace 1998; Lebreton et al. 2006). The Debye lengths in the Mars ionosphere can be as small as ~ 3 mm and as large as ~ 1 m in the regions of scientific interest. The current collection is primarily orbit limited (the radius of the sensor is ~ 3.175 mm) except in regions of the highest density, where the current collection can be partially sheath limited.

The stub is a 5 cm by 1.15 cm region at the base of the sensor and includes the disk of the preamplifier case that faces the sensor. The stub is electrically isolated from the sensor

and the rest of the preamplifier case. The surface is biased by the BEB to the sensor voltage plus a programmable offset between -9.8 V and 9.8 V. The bias voltage offset is slated to be positive (~ 1 V) so that photoelectron fluxes from the stub are not attracted to the sensor.

The “guard” is a $10\text{ cm} \times 3.2\text{ cm}$ cylinder that houses the preamplifiers. Its outer surface is coated with a black nickel, which makes a conducting surface and has thermal properties that maintain the preamplifier within its operating temperature. The guard surface, exposed to the plasma is also biased by the BEB to the sensor potential plus a programmable offset between -9.8 V and 9.8 V. In flight, the guard voltage is slated to be -1 V to reflect photoelectrons from boom and spacecraft. Photoelectrons from the guard cannot travel in a straight path to the sensor since the disk at the outer end of the preamplifier case is slightly larger in diameter. The guard and stub are designed to electrically isolate the sensor from the spacecraft. The voltages applied to the guard and stub surfaces are fine-tuned after the booms are deployed to optimize the LP and wave measurements in Mars’ ionosphere.

Titanium nitride (TiN) is used on the surface of the sensor because it has shown to be chemically resistive to atomic oxygen erosion (Wahlström et al. 1992), whereas DAG213 (graphite/epoxy), used on previous instruments, is known to have a finite life due to erosion by atomic oxygen. Mars’ ionosphere is abundant in atomic oxygen, which reacts strongly with carbon. The erosion can lead to changes in surface properties such as photoelectron yield and resistance. In addition, a TiN coating has a low work-function variation of the surface enabling measurements of small T_e .

However, TiN has poor thermal properties. In sunlight (at Mars) and heat induced by atmospheric drag, the surface is expected to have temperatures on the order of 180°C . For this reason, a thick coat ($\sim 50\ \mu\text{m}$) of DAG213 is baked onto the boom surface instead to maintain a suitable thermal environment for the wire harness. Photoelectron emission and resistance of the boom is not critical to the LPW experiment.

2.2.3 Preamplifier Design

Figure 7 displays a block diagram of the preamplifier electrical design. The sensor is the input. The waves preamplifier is a voltage follower (OP16) with unity gain, similar to those on FAST (Ergun et al. 2001), Polar (Harvey et al. 1995), and THEMIS (Bonnell et al. 2008). A current bias, controlled by the BEB, ranges from $-1\ \mu\text{A}$ to $1\ \mu\text{A}$ and is set to optimize the coupling between the sensor and the plasma. The input resistance to the wave preamplifier is $>10^{12}\ \Omega$ and the input capacitance is $\sim 3\ \text{pF}$. The frequency response of the three bands including the preamplifier response, analog filters, and signal processing is displayed in Fig. 8.

A relay controls the electrical connection between the sensor and the preamplifiers. When connected to the LP preamplifier, the probe takes the same potential as the positive input of the LP amplifier.

The LP preamplifier is an inverting amplifier converting the probe current to a voltage signal through a $50\ \text{k}\Omega$ resistor. It measures currents from $-0.2\ \text{mA}$ to $0.2\ \text{mA}$ with a precision of $\sim 0.8\ \text{nA}$. The waves preamplifier incorporates an OP16 operational amplifier with high input impedance ($>10^{12}\ \Omega$) and low leakage currents ($<100\ \text{pA}$).

The power supplies of both of the preamplifiers are “floating”. The ground ($<100\ \text{Hz}$) level of the $\pm 12\ \text{V}$ supplies is at the output of the waves preamplifier when in waves mode, and at the sweep voltage when in LP mode. The floating power supplies allow the LP and waves preamplifiers to operate over a large voltage range of V_{SC} with respect to the plasma.

Fig. 7 Simplified schematic of the LWP preamplifiers. The relay is shown in the LP setting. The guard and stub voltages (not shown) are directly attached to the preamplifier case

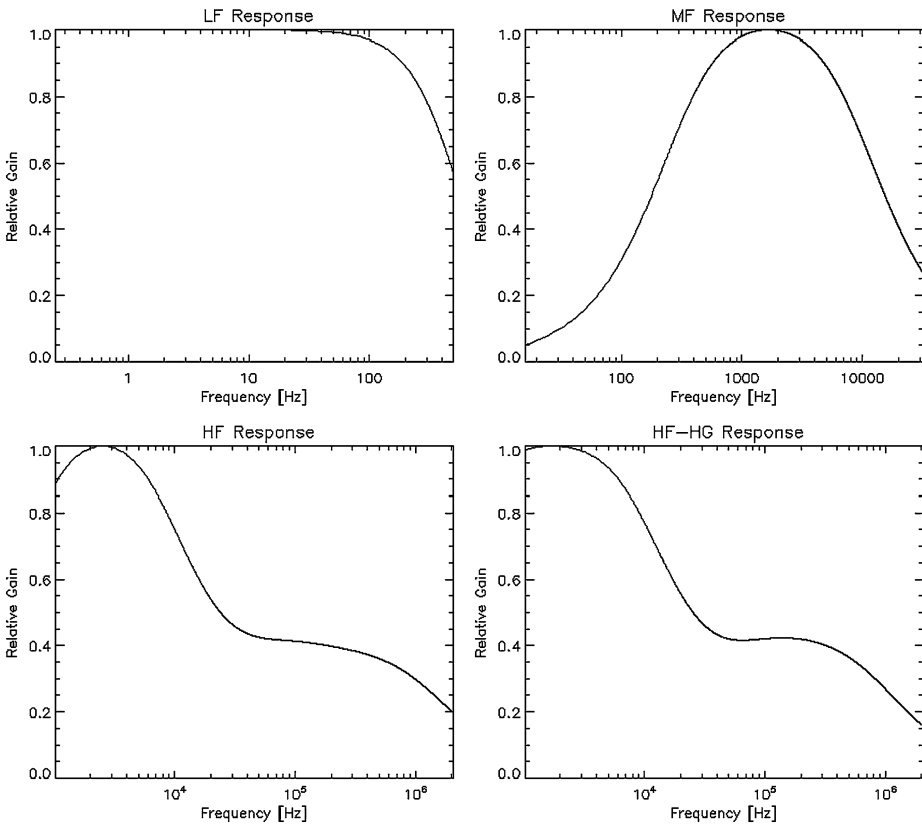
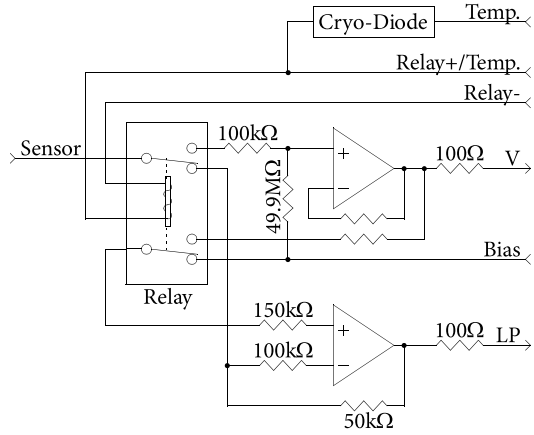


Fig. 8 The gain versus frequency for the different LWP frequency bands (LF, MF, and HF). The high frequency range has two different gain stages (HF and HF-HG)

3 Control Electronics

The signal-processing unit for the LPW instrument contains two circuit boards, the Boom Electronics Board (BEB) and the Digital Fields Board (DFB), which are located in the PFDPU. The LP and waves preamplifiers on the 2 booms and the EUV sensors are connected to the BEB or DFB as illustrated in Fig. 1. The LPW commands arrive via the PFDPU and data packets from the LPW are sent to the PFDPU for transmission (survey data) or stored in the archive location in the PFDPU for possible transmission later (archive data).

The LPW, once configured, operates the sweeps and cycles through the measurements independently. The spacecraft controls the one time boom deployment, the one time EUV door deployment, and the heaters on the EUV and the boom. The spacecraft provides alerts to the PFDPU for the LPW. The PFDPU holds configuration tables for the LPW in EEPROM. The PFDPU also passes operation commands to the LPW and maintains the archive memory. The PFDPU controls the EUV aperture.

3.1 Boom Electronics Board

The MAVEN LPW utilizes a single, centralized the Boom Electronics Board (BEB) mounted in the PFDPU. The BEB hosts the analog preamplifier and sensor control circuitry that sets LP sweeps, sets the current biases in waves mode, switches the relay between LP and waves mode, controls the voltages on surfaces close to the LP and the waves sensor (called guards and stubs), supplies floating power to the preamplifiers, and operates the temperature diode on the preamplifier board. The BEB also receives the LP and waves signals from the preamplifier and filters these signals before passing them to the DFB.

A simplified block diagram of the BEB is displayed in Fig. 9. Since there are two boom/preamplifier/sensor units, the BEB has two nearly identical sides that run independently; side 1 controls boom 1 and side 2 controls boom 2. Only one side is diagrammed in Fig. 9. The signal processing that creates the electric field or wave signals is also located on the BEB.

The floating ground drivers (Fig. 9) are at the heart of the BEB architecture. The floating ground drivers, which operate from ± 90 V power supplies, create a unique ground reference for each of the sensors. In this way, the sensors have a wide operating range and can operate when the spacecraft is charged with respect to the plasma. The grey area in Fig. 9 represents the circuitry on the floating ground.

3.1.1 LP Mode Functions

In LP mode, the sensor is connected to the LP preamplifier by the relay (Fig. 7). The BEB switches in Fig. 9 are shown in LP mode. The bias/sweep driver is controlled by a 12-bit digital to analog converter (DAC), which in turn is controlled by the DFB. The DAC output is amplified to a maximum range of ± 50 V with a step size of ~ 24 mV. In LP mode, the output of the bias/sweep driver (run from ± 90 V supplies) controls the potential of the sensor or the “sweep” potential via the LP preamplifier (Fig. 7). As described later, sweeps are digitally stored in configurable tables of DAC values from 0 to 4097.

The bias/sweep driver output also controls the floating ground driver (Fig. 9) input. The floating ground driver is a unity-gain, high voltage (± 90 V) amplifier that de-couples the BEB circuitry from the spacecraft ground. In turn, the charge pump (Fig. 9) power supplies create ± 12 V power referenced to the floating ground. The “floating power” from the charge pumps operates the preamplifiers and some of the BEB circuitry. The guard and stub

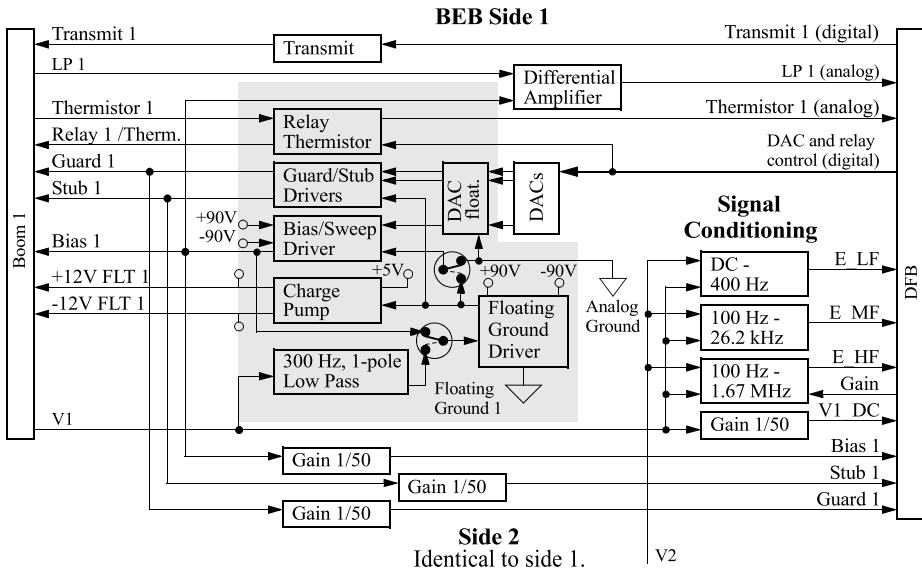


Fig. 9 A simplified function diagram of the boom electronics board (BEB). There are two identical sides to the BEB. Side 2 is not displayed. The grey area represents the circuitry on a floating ground

Table 1 The ranges and resolution of the floating ground, bias, guard, and stub settings

LP mode	Operation	Nominal range	Step	Reference
Floating ground	Sweep	± 90 V	N/A	Sweep
Bias/sweep	Sweep	± 50 V	24.4 mV	Analog ground
Guard	Guard	± 9.8 V	5.86 mV	Floating ground
Stub	Stub	± 9.8 V	5.86 mV	Floating ground
Waves mode	Operation	Nominal range	Step	Reference
Floating ground	Waves	± 90 V	N/A	W preamplifier
Bias/sweep	Bias	± 1 μ A	0.49 nA	Floating ground
Guard	Guard	± 9.8 V	5.86 mV	Floating ground
Stub	Stub	± 9.8 V	5.86 mV	Floating ground

potentials are independently set to a value between -12 V to $+12$ V (step size of ~ 6 mV) referenced to the floating ground by two additional DACs. All DACs are controlled by the DFB. Table 1 describes the outputs of the BEB drivers.

During a LP sweep, the bias/sweep DAC is stepped through a series of values in a sweep table. The BEB and LP circuitry is designed to settle in less than 7.8 ms so that 128 steps can be made in one second. In LP mode, the waves preamplifier (of the sensor that is in LP mode) simply returns the value of the sweep potential.

3.1.2 Waves Mode Functions

In waves mode, the sensor is connected to the waves preamplifier (Fig. 7) and the BEB switches in Fig. 9 are set to the opposite position that is displayed in the diagram (dashed lines in Fig. 7). The input to the floating ground driver is the DC (to 300 Hz) level of the

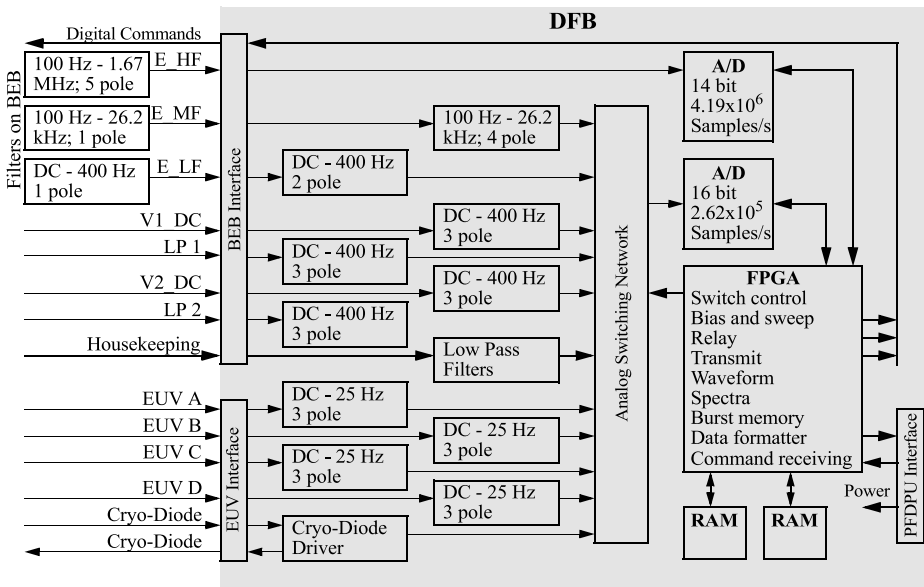


Fig. 10 A block diagram of the DFB. The DFB is shown in the *grey area*. The filters on the left are located on the BEB (see Figure 9)

waves preamplifier signal, allowing for an extended range of DC voltages on the sensor (± 90 V). In turn, the floating power (from the charge pumps), the stub, and the guard voltages are referenced to the DC level of the waves preamplifier. The bias/sweep driver is also referenced to the floating ground. Its output can be adjusted to ± 50 V with respect to the floating ground. In combination with the 49.9 M Ω resistor in the waves preamplifier (Fig. 7), a high-impedance bias current is flowed to the sensor with a range of approximately ± 1 μ A.

The BEB includes signal conditioning for the wave and DC electric fields. This conditioning (Fig. 9) sets three frequency bands for the power spectra. The high-frequency band (100 Hz to 1.62 MHz) has a gain option, allowing for an increase in gain by 5. Since electric fields are not obtained during LP sweeps, the DC electric field is piecewise continuous. Other functions of the BEB include relay drivers to activate the relays on the preamplifiers, circuitry to support the temperature diodes on the preamplifiers, and a simple amplifier for transmitting white noise using the stacer elements. The transmitters are operational amplifiers with a range of ± 5 V. The transmitted power is less than 100 μ W.

3.2 Digital Fields Board

The Digital Fields Board (DFB; Fig. 10) receives analog signals from the two LP and waves sensors via the BEB and receives the analog signals from the EUV sensors. It performs analog signal conditioning, the analog to digital conversion, and digital signal processing on the scientific and engineering signals inside of a field-programmable gate array (FPGA, Actel RTAX2000). The DFB also digitally controls the relays, guards, stubs, and sweep and bias of the LP and the waves preamplifiers. It creates white noise signals for transmission as well.

Table 2 The low-pass poles of the analog filters. All filters are designed to have linear phase delay (Bessel) so that the signal shape is preserved. The E_{MF} and E_{HF} signals have a 1-pole high pass filter at 100 Hz

Signals	Filter freq.	Poles	Sample rate (s^{-1})	Signals	Filter freq.	Poles	Sample rate (s^{-1})
LP _{1,2}	400 Hz	3	16,384	EUV_A	25 Hz	3	1024
V _{1,2}	400 Hz	3	1024	EUV_B	25 Hz	3	1024
E_{LF}	400 Hz	5	1024	EUV_C	25 Hz	3	1024
E_{MF}	26.2 kHz	5	65,536	EUV_D	25 Hz	3	1024
E_{HF}	1.62 MHz	5	4.19×10^6	EUV T	25 Hz	3	1024
Guard _{1,2}	25 Hz	3	1024	Bias _{1,2}	25 Hz	3	1024
Stub _{1,2}	25 Hz	3	1024	Temp _{1,2}	25 Hz	3	1024

3.2.1 Signal Conditioning and A/D Conversion

The DFB receives and conditions the science and engineering signals listed in Table 2 for A/D conversion. All signals are conditioned by Bessel filters. Two A/D converters are employed. The E_{HF} signal is converted by a 14-bit A/D at 4.19×10^6 samples/s. All of the other channels share a 16-bit A/D operating at 262,144 samples/s. The signals are channeled to the A/D via a series of analog switches controlled by the FPGA.

3.2.2 Signal Processing: Waveforms and Burst Memory

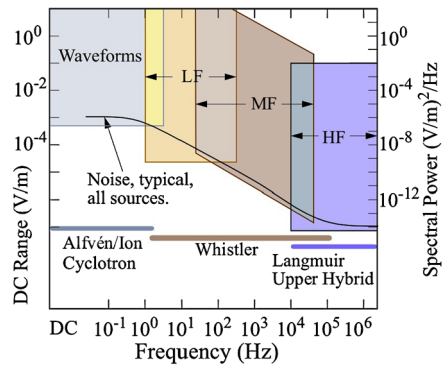
The A/D data are input to the FPGA for signal processing, compression, and packaging for telemetry transmission. External RAM is added for data storage during the processing. The waveform signals undergo simple averaging for data reduction. The EUV signals, filtered at 25 Hz and sampled at 16 bits, 1024 times a second, are averaged over a one-second period. A 20-bit value is reported. The A/D converter has 1/4 least significant bit (LSB) accuracy with ~ 1 LSB random noise. The averaging reduces the noise to $< 1/4$ LSB. Calibrations indicate that the 18 most significant bits are reliable.

The LP signals are filtered at 400 Hz and sampled at a rate of $16,384 s^{-1}$. The sampling is synchronized with the sweep steps. The oversampling allows for averaging of 16 samples in a ~ 1 ms period at the end of a sweep step, giving the LP preamplifiers ~ 7 ms of settling time. A 20-bit value is reported. Again, calibrations indicate that the 18 most significant bits are reliable.

The E_{LFDC} , V_1 , and V_2 signals are averaged to 64 samples/s with 16 bits reported. The notation ‘DC’ is added to separate this 64-point measurement per subcycle from the burst data. DC data are piecewise continuous. The E_{LF} , E_{MF} , and E_{HF} waveforms are directed to a burst memory, which stores intervals of 1024 samples of E_{LF} waveform and 4096 samples of E_{MF} , and E_{HF} waveforms. The short intervals of “burst” data are transferred to the PFDPU as archive data. Portions of the archive data can be later transmitted.

The burst intervals are selected based on the amplitude of the waveforms. An algorithm (in the FPGA) identifies the peak absolute amplitude in sixteen, 256-point intervals over the 4096 samples for each of the E_{MF} and E_{HF} waveforms, and sixteen 64-point intervals over the 1024 samples of the E_{LF} waveform. The highest four of the sixteen peaks are averaged to assign a value representing the data quality. This algorithm captures single spikes (e.g. dust impacts) with a moderate reduction in data quality, but favors multiple spikes (e.g. electron phase-space holes or double layers) and sinusoidal waveforms (e.g. Langmuir waves). The

Fig. 11 The frequency range of the electric field waves measurement. The lowest frequencies are recorded as waveforms (E_{LF}). Higher frequencies (the LF, the MF, and the HF frequencies bands) are recorded as spectra and, when operated in burst mode, as short bursts of waveforms (E_{LF} , E_{MF} , and E_{HF})



intervals with the highest data quality are transferred to the PFDPU archive once every master cycle (configurable). The intervals of E_{LF} , E_{MF} , and E_{HF} waveforms are selected independently. The burst data within the PFDPU archive are selected for transmission by ground command after examination of spectra.

3.2.3 Signal Processing: Spectra

The spectral processing on MAVEN is derived from that used on THEMIS (Cully et al. 2008). Piecewise continuous sets (multiples of 1024 points) of each type of data (E_{LF} , E_{MF} , and E_{HF}) are acquired into a memory during a sub-cycle (typically 1 s, see below). After acquisition, the piecewise continuous 1024-points sets are each processed with a Fast Fourier Transform (FFT). The E_{LF} signal (1024 samples/s) may have only one 1024-point data set in a sub-cycle (1 s). 4096 values are collected for each of the E_{MF} and E_{HF} signals in a sub-cycle. The four FFTs are averaged to provide better dynamic range.

The FFT operation is internal to the FPGA. The processing first applies a Hanning window, followed by the FFT. The FPGA has a built-in arithmetic processing unit that performs the “butterfly” operation at the heart of the FFT. After the FFT, the powers in 512 frequency bins are calculated and averaged. The frequency bins are then combined to give pseudo-logarithmic frequency spacing ($\delta f/f$). The E_{HF} channel is reduced to 128 bins with $\delta f/f \sim 3.1\%$ (ranging from 2.1% to 4.1%) in the range of 100 kHz to 2.1 MHz so that narrow band emissions can be fit to an accuracy of $\delta f/f \sim 1\%$, allowing for an accurate determination of plasma density from $\sim 100 \text{ cm}^{-3}$ to $\sim 4 \times 10^4 \text{ cm}^{-3}$. The E_{MF} and E_{LF} spectra have 56 bins each with $\delta f/f \sim 9\%$. Table 3 summarizes the frequency and amplitude ranges of the spectral processing. Figure 11 displays the spectral coverage of the waves.

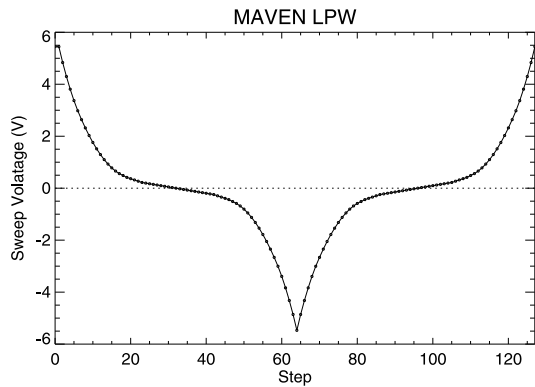
3.2.4 Signal Processing: Data Compression

The data are compressed with several methods. Waveform data undergo “delta” compression. Under this algorithm, data from a specific waveform are grouped in sets of 32 words (a word is 16 bits for most signals and 20 bits for LP and EUV signals). The first word is reported in full. The difference between the remaining 31 words is then reported with as few bits as needed so that no information is lost. The needed number of bits is reported in the field as well. This type of lossless compression typically results in reduction to 25%–50% of the original data volume during quiet periods, with less efficient reduction during active periods. The spectra undergo a pseudo-logarithmic compression to an 8-bit number representing over 140 dB of range at $\sim 5\%$ accuracy.

Table 3 Characteristics of the E_{LF} , E_{MF} and E_{HF} spectra. The noise figures do not include sources from the spacecraft. Solar array noise, which will be determined once on orbit, may degrade performance

Signal	Gain	Analog filtering		Digital processing			Power spectral density					
		Low pass -3 dB (Hz)	High pass -3 dB (Hz)	Sample rate (s^{-1})	Freq. min. (Hz)	Freq. max. (Hz)	# freq. bins	($\delta f/f$) ave.	($\delta f/f$) min.	($\delta f/f$) max.	Receiver sensitivity ($(V/m)^2/Hz$)	Narrow band range ($(V/m)^2/Hz$)
E_{LF}		DC	400	1024	0.5	7.5	8	$\delta f = 1$ Hz			8×10^{-12}	6×10^{-2}
E_{MF}		100	2.6×10^4	6.6×10^4	8.5	496	48	9 %	6.5 %	12 %	3×10^{-12}	6×10^{-2}
E_{HF}	Low	100	1.6×10^6	4.2×10^6	544	3.2×10^4	48	9 %	6.5 %	12 %	5×10^{-15}	4×10^{-5}
	High	100	1.6×10^6	4.2×10^6	2048	9.6×10^4	24	$\delta f = 4096$ Hz			2×10^{-15}	4×10^{-5}
					1×10^5	2.1×10^6	104	3.1 %	2.1 %	4.1 %	10^{-15}	2×10^{-6}
					2048	9.6×10^4	24	$\delta f = 4096$ Hz			5×10^{-16}	2×10^{-6}
					1×10^5	2.1×10^6	104	3.1 %	2.1 %	4.1 %	10^{-17}	10^{-7}
											2×10^{-17}	10^{-7}

Fig. 12 A pseudo-logarithmic, bi-directional LP sweep slated for Mars' ionosphere. The sweep is bidirectional to detect hysteresis. The steps are $\sim 10\%$ when $|V| > \sim 0.35$ V. If $|V| < \sim 0.35$ V, the steps are at the finest level (24.4 mV)



3.2.5 LP Sweep Generation

The LP sweep is generated from one of 16 tables stored inside of a RAM. Each sweep table contains 128 12-bit integers that are sent to the DACs on the BEB (see Fig. 9). The DAC circuitry is designed to have a -50 V to 50 V range with 24.4 mV resolution. The sweep tables are fully programmable. The sweep is executed at the beginning of the sub-cycle (see Fig. 3). The dwell time per step is $1/128$ of the sub-cycle period. In other words, the sweep takes the entire sub-cycle. In the ionosphere, the sub-cycle is expected to be 1 s, so the dwell time is ~ 7.8 ms. In the solar wind, the sub-cycle is slated to be 16 s resulting in $1/4$ second dwell times.

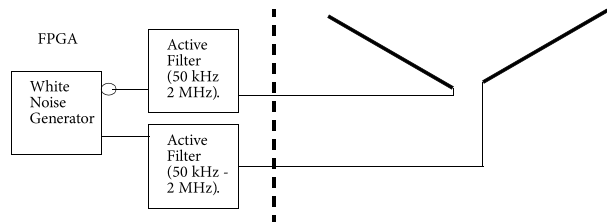
The sweeps for the initial operation of the LPW are bi-directional with pseudo-logarithmic steps. The sweep in Fig. 12 is slated for Mars' lower ionosphere. It starts at ~ 5.5 V, steps down to ~ -5.5 V, then returns to 5.5 V. The downward and upward current-voltage measurements can be compared to detect hysteresis, which can be from changes in the surface properties of the sensor, rapid changes in plasma conditions, or rapid changes the spacecraft potential. Viewing the left side of Fig. 12, the sweep steps are roughly -10% ($\delta V_{swp}/V_{swp}$), where V_{swp} is the programmed sweep potential. At step 20 (on horizontal axis), $|\delta V_{swp}|$ is ~ 24.4 mV, which is the smallest step size. The fine stepping near zero voltage allows for an accurate determination of T_e (e.g. Brace et al. 1973).

An important feature of the MAVEN LPW is the zero-crossing adjustment algorithm. The algorithm, part of the FPGA design, identifies the potential (V_{zero}) at which the probe current (I_p) is such that $|I_p - I_{offset}|$ has the lowest absolute value within a sweep. I_{offset} is a programmable offset that represents the best current level to measure T_e . After filtering and limiting V_{zero} , the subsequent sweep is adjusted so that the applied potential on the LP is determined by $V_{lp} = V_{swp} - V_{zero}$. The zero-crossing algorithm is designed so that fine stepping is in the critical region near $I_p = 0$ since the curvature in the $I-V$ characteristic near (or slightly above) $I_p = 0$ is important for determining T_e . Essentially, this algorithm adjusts for spacecraft potential variations. The zero-crossing adjustment is restricted by setting a maximum and minimum of V_{zero} or it can be disabled.

3.3 Relaxation Sounding

The basic idea of relaxation sounding is to stimulate Langmuir waves locally, determine the plasma frequency (ω_{pe}) and derive the plasma density (Etcheto et al. 1981). Naturally occurring Langmuir waves are expected to be infrequent. The FPGA includes a random

Fig. 13 A block diagram of the LPW relaxation sounder



digital signal generator at 8.39 MHz. The resulting digital signal (3.3 V) has a white noise spectrum. This digital signal is amplified and filtered on the BEB. The positive signal is fed to the stacer element of LP1 (Fig. 13). An inverted signal is fed to the stacer element of LP2. The signals are broadcast for ~ 15 ms. After a programmable delay (slated to be < 1 ms), spectra are collected in all electric field bands (see Sect. 3.2.3). The E_{HF} waveform has 4096 points at 4.19 M samples/s., representing 2 ms of data. The rapid capture is required so that the plasma waves do not experience significant damping. The broadcast power is expected to be $\sim 100 \mu\text{W}$.

The stacer elements, ~ 7.1 m in length, are expected to stimulate the normal modes of the plasma at wave vectors of $k \sim 0.5 \text{ m}^{-1}$. Langmuir waves are expected to have frequencies of:

$$\omega^2 = \omega_{pe}^2 + 3v_{the}^2 k^2$$

where $\omega_{pe}^2 = ne^2/\epsilon_0 m_e$ is the plasma frequency. Here, v_{the} is the electron thermal speed, n is the plasma density, e is the electron charge, and m_e is the electron mass. T_e in Mars' ionosphere is expected to be between 0.1 eV and 0.3 eV so the second term on the right hand side ($3v_{the}^2 k^2$) is considerably less than the first term. Furthermore, the magnetic field (B) rarely exceeds a few hundred nT. Therefore, the electron cyclotron frequency is considerably less than ω_{pe} , so corrections for upper hybrid mode stimulation are not required.

3.4 Calibration

The LPW was calibrated in subsections and end-to-end. The BEB and preamp, which operate as a unit, were calibrated as one subsection. The sensor/preamp and BEB calibration used a resistor network to simulate the various plasma conditions. The waves calibration used Faraday cage and resistor network. The DFB was characterized independently by stimulating its inputs. Finally, the LPW is recalibrated end-to-end, stimulating the sensors and recording the output. The subsection transfer functions, preamp/BEB and the DFB were compared to end-to-end transfer functions. These calibrations are supplemented with in-flight calibrations described below.

4 LPW Operations

Since the LPW sensors cannot operate in LP mode and wave mode simultaneously, the LPW instrument cycles between the LP mode and waves mode (Sect. 1.3). A master cycle (Fig. 3) is defined to contain four sub-cycles. The sub-cycles are planned to be: (a) LP sweep on probe 1, (b) passive electric field wave measurements, (c) LP sweep on probe 2, then (d) relaxation sounding. The master cycle length can be configured to be from 4 s (1 s sub cycles) to 256 s (64 s sub-cycles). The sub-cycle activity within a master cycle also

Table 4 The 16 mode configurations loaded for MAVEN's launch. Waves-P and waves-A the Bias/Stub/Guard settings are "A": +25 nA/0 V/ - 5 V and for "B": 0 nA/0 V/0 V. LP1 and LP2 settings are "A": 0 V/- 5 V and for "B": 0 V and 0 V

Mode	Description location/sun		LP sweep range (V) and direction		Bias stub guard	Master cycle length (s) and sequence	Data rate survey/archive (bits per s)	
0	Deep dip	Yes	-5.45 to 5.45	BiDir	A	4 LP1; P; LP2; A	3019	5010
1	Low altitude	Yes	-11.0 to 11.0	BiDir	A	4 LP1; P; LP2; A	3019	5010
2	Mid altitude	Yes	-20.9 to 20.9	BiDir	A	16 LP1; P; LP2; A	811	0
3	High altitude	Yes	-40.3 to 40.3	BiDir	A	128 LP1; P; LP2; A	165	0
4	Deep dip	No	-11.0 to 11.0	BiDir	B	4 LP1; P; LP2; A	3019	5010
5	Low altitude	No	-20.9 to 20.9	BiDir	B	4 LP1; P; LP2; A	3016	5010
6	Mid altitude	No	-20.9 to 20.9	BiDir	B	16 LP1; P; LP2; A	811	0
7	Transition	N/A	-40.3 to 40.3	BiDir	B	8 LP1; P; LP2; A	3100	0
8	Dust	N/A	0	N/A	0	256 P; Null; P; Null	90	270
9	Cleaning	Yes	0	N/A	0	256 P; P; P; P	58	0
10	Cruise	Yes	-50.0 to 50.0	BiDir	0	256 LP1; P; LP2; A	50	0
11	Test 0	N/A	N/A	N/A	0	4 N/A	3019	5010
12	Test 1	N/A	N/A	N/A	0	8 N/A	1622	5010
13	Test 6	N/A	N/A	N/A	0	256 N/A	165	0
14	Test 7	N/A	N/A	N/A	0	4 N/A	58	0
15	Test 15	N/A	N/A	N/A	0	8 N/A	1622	5010

can be configured, within limitations of data rates and spectral processing capabilities. For example, the LPW could perform continuous sweeps by programming all sub-cycles to LP sweeps.

4.1 Operating Modes

The LPW is able to store sixteen configurations or "modes" in RAM. The stored modes at launch are listed in Table 4. These configurations include settings for the LP sweep tables, bias currents, guard voltages, stub voltages, master cycle length, master cycle usage, and data rate configurations. Several of the modes are designed for the 9 month cruise during which the LPW booms are not deployed. Other modes are for testing the instrument performance. After orbital insertion and the LPW booms are deployed, we intend to replace the cruise and some of the engineering modes with appropriate science modes. The flexibility of the LPW design allows MAVEN scientists to focus on specific science tasks.

To ensure that the LPW instrument is not impacted by nor is affecting other instruments or the spacecraft, several additional instrument settings are built in to the design. All the PF instruments operate with the same clock. The particle instrument energy sweeps and the LP potential sweeps start times are synchronized. Delays can be configured if interference is detected. The most significant known noise source of the spacecraft is expected to be from solar panel switching. The magnitude of this noise is unknown prior to LPW boom deployment. To avoid this noise, the LPW wave receivers can be configured to operate between periods of solar array switching (see Sect. 4.3). Finally, LPW's active broadcasting signal can be enabled or disabled to avoid impacting other instruments.

A new science mode, the dust detection mode, has been added to measure the dust flux from comet C/2013 A1 (Siding Spring), due to pass Mars on October 19, 2014, roughly one

month after MAVEN is expected to arrive. The LPW instrument is configured as a single-antenna wave instrument. The HSBM is set to trigger on the electric field signature of dust impacts such as done on the STEREO (Meyer-Vernet et al. 2010) and the Wind satellite (Malaspina et al. 2014). The impact rate on the spacecraft allows for an estimate of the impacts on Mars' upper atmosphere.

At launch the LPW orbit-averaged data rate allocation is 708 bits/s. This data rate allows the LPW instrument to be operated at periapsis (<500 km altitude) in 4 seconds master cycle, at the mid-altitudes (500–2000 km) in 16 seconds master cycle, and at >2000 km altitudes in 128 second master cycle. Since launch, the telemetry allocation has significantly increased, allowing the LPW to operate in a 4 second master cycle, the fastest cadence of the instrument, in much of the mid-altitude part of the orbit. The modes in Table 4 will be updated after arrival at Mars to take advantage of increase telemetry volumes.

4.2 Surface Control

The bias, guard, and stub setting (Table 4) are to be adjusted to optimize the LPW performance once on orbit. This optimization is performed in early commissioning and roughly once a month afterward. The bias, guard, and stub settings are stepped through a set of values while taking data. The data from each setting is analyzed for accuracy, noise performance, and stability after which the new tables are commanded.

An instrument mode was developed so that the sensor surface (TiN) periodically can dwell at the highest (+50 V) and lowest (−50 V) potentials. This process of surface cleaning has been reported in previous LP instruments (Krehbiel et al. 1981; Brace 1998). Hysteresis in the I – V characteristics, that is differing values when sweeping positive than when sweeping negative, is an indication of possible surface contamination.

4.3 Solar Array Noise

The solar arrays on the MAVEN spacecraft have the potential to create high-frequency electromagnetic signals, especially coming out from shadow. As part of the electromagnetic control plan, the MAVEN solar arrays avoid switching for 1/2 of a second every second. The LPW instrument is designed to measure high-frequency waves for 1/2 second during the quiet period.

5 Data Products

5.1 Data Quantities

The data products produced by the LPW instrument are in Table 5. The products from the Langmuir sweep are derived from a fit to the I – V characteristic (Wahlund et al. 2005). The default fitting routine includes one electron population (temperature), an ion current with ram velocity, the spacecraft potential, the photoelectron current from the spacecraft, and the photoelectron current from the sensor. Multiple electron and ion populations may be considered in special cases as done in the CASSINI satellite encounter with Titan (Wahlström et al. 1992). The LP density is cross calibrated with the active sounding determination of the electron density. E_{LFDC} is produced and stored in piecewise continuous periods. The power spectral densities of the three bands of electric field waves are combined.

Table 5 The science quality products archived at the NASA PDS center. The first letters in the PDS production name indicate from which instrument function the product is created from: Waves mode (w), Sweep mode (lp), and where data is merged from both modes or other sources (mrg)

PDS products	Description
mrg_sc_pot	The spacecraft potential based on observations from all 4 sub-cycles.
w_e12	E_{LFDC} Low frequency (DC–32 Hz for master-cycle of 4 seconds) electric field measurements at 64 samples from every other sub-cycle.
w_e12_burst_lf	E_{LF} Burst LF data: Intervals of data (DC–500 Hz; 1024 samples/s; 16 bits) that are triggered on amplitude. Only a small portion of these data can be transmitted. These data come from the passive sub-cycle.
w_e12_burst_mf	E_{HF} Burst MF data: Intervals of data (100–8000 Hz; 16,384 samples/s; 16 bits) that are triggered on amplitude. Only a small portion of these data can be transmitted. These data come from the passive sub-cycle.
w_e12_burst_hf	E_{HF} Burst HF data: Intervals of data (100 Hz – 1.6 MHz; 2^{22} samples/s; 14 bits) that are triggered on amplitude. Only a small portion of these data can be transmitted. These data come from the passive sub-cycle.
w_spec_pas	The LF, MF, and HF spectra merged into one spectrum from passive sub-cycle.
w_spec_act	The LF, MF, and HF spectra merged into one spectrum from active sub-cycle.
w_n	The electron density based on HF-spectra when Langmuir line is detectable.
lp_iv	Current-Voltage sweeps from both booms; the cadence is every other sub-cycle (Fig. 3).
lp_n_t	The electron temperature and density based on the IV-curves and when available adjusted based on wave density, data from every other sub-cycle (Fig. 3).
mrg_poynting_flux	Derived using L2 magnetometer data and electric field (E_{LFDC}).

6 First Data

The MAVEN satellite successfully launched on November 18, 2013. The LPW instrument is operating as expected with stowed booms. Figure 14 displays examples of from the early orbit at Mars. These data are not fully calibrated. The example data from the cruise is from a time period when the spacecraft did a sun-directed cruciform scan. The instrument was in solar wind mode, Mode 3 described in Table 4. The scan caused the two sensors to be partially shadowed at different times and to different fractions. Each sensor detects the local plasma density and temperature. The wave spectra close to the spacecraft is quiet (Fig. 14a) Just prior to the cruciform, at ~04:55 UT, the instrument was power cycled. This resulted in a reset of the automatic offset adjustment to zero. Subsequently, the automatic zero-crossing algorithm slowly moved the IV-sweep to a positive voltage offset demonstrating the algorithm working. Finally, Fig. 14c displays the potential from sensor 1 in the PAS sub-cycle. Figure 14 is produced with preliminary calibration values.

7 Summary

The LPW instrument is designed to measure the n_e and T_e and to measure the spectral power density of waves in Mars' ionosphere. Table 6 summarizes the LPW mass, power, and telemetry and Table 7 summarizes the expected instrument performance. The LPW instrument utilizes two, 40 cm long by 0.635 cm diameter cylindrical sensors, which can be configured to measure either plasma currents or plasma waves. The sensors are mounted on two, ~7.1 meter long stacer booms. The sensors and nearby surfaces are controlled by a

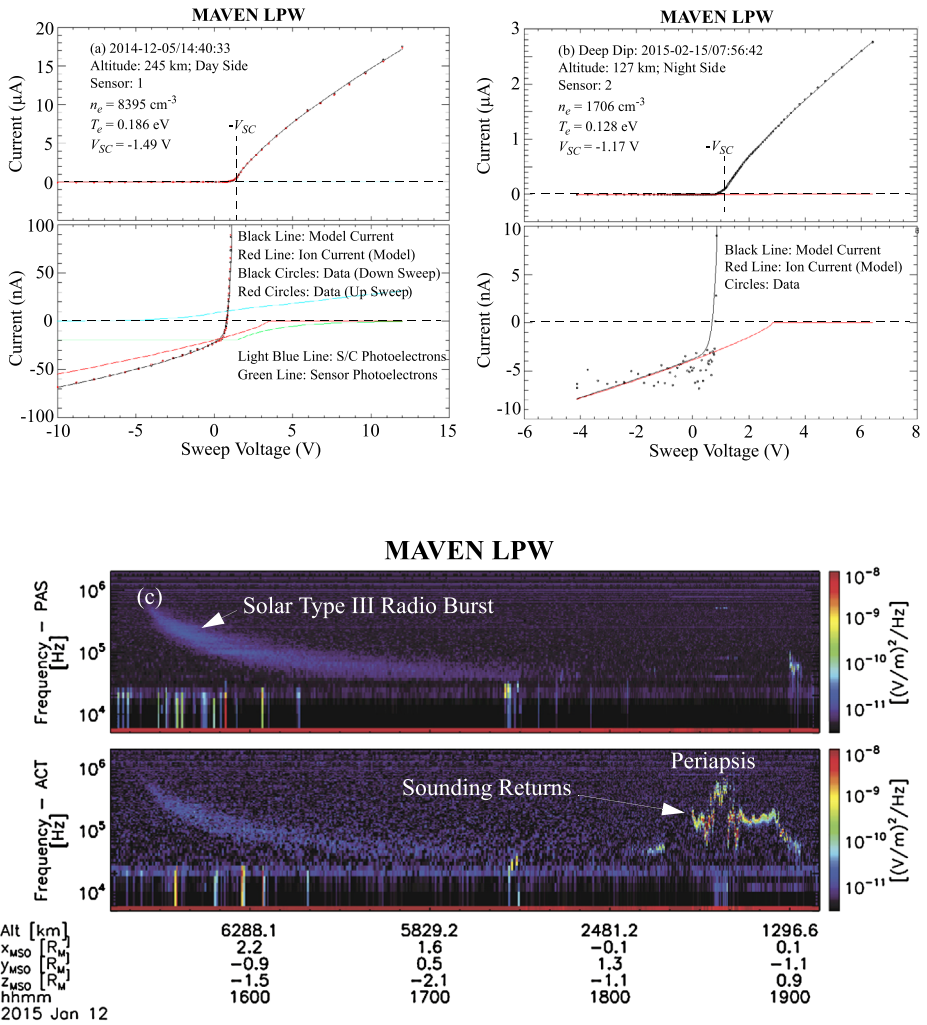


Fig. 14 (a) An example of a dayside sweep from the MAVEN LPW. The red and black circles are data. The red and black lines represent fits. (b) An example of data from the deep dip campaign in February 2015. (c) Passive (top) and active (bottom) wave spectra over the same time period. The wave spectra have lower noise as they have longer averages. One can see a solar type II radio burst signal on the right of each spectra. The active spectra show Langmuir wave returns near periapsis, which allow for accurate determination of the plasma density

Table 6 The LPW instrument’s resource use

Resource	Value
EUV (incl harness)	1.4 kg
LPW boom and sensor mass (2)	2.6 kg
DFB and BEB mass	0.98 kg
Total Mass	4.98 kg
Power (incl EUV)	2.7 W
Normal total data rate	711 bps
Maximum data rate (survey)	3100 bps
Maximum data rate (archive)	5010 bps

Table 7 The expected instrument performance for different environment

N_e accuracy		LPW sweep		Spectra ACT/PAS
		Relative accuracy	Absolute accuracy	Absolute accuracy
$n_e \geq 10^3 \text{ cm}^{-3}$ $T_e \geq 0.1 \text{ eV}$	Daylight/shadow	5 %	20 %	2 %–4 % (n_e only)
$n_e \geq 10^2 \text{ cm}^{-3}$ $T_e \geq 0.2 \text{ eV}$	Daylight	10 %	40 %	6 %–12 % (n_e only)
$n_e \geq 10^2 \text{ cm}^{-3}$ $T_e \geq 0.2 \text{ eV}$	Shadow	5 %	20 %	6 %–12 % (n_e only)
$n_e \geq 10^1 \text{ cm}^{-3}$ $T_e \geq 0.5 \text{ eV}$	Daylight	50 %	Factor of 2	6 %–12 % (n_e only)
$n_e \geq 10^1 \text{ cm}^{-3}$ $T_e \geq 0.5 \text{ eV}$	Shadow	25 %	Factor of 2	6 %–12 % (n_e only)

Boom Electronics Board (BEB), which allows for operation as either a Langmuir Probe or a wave electric field receiver. The Digital Fields Board (DFB) conditions the analog signals, converts the analog signals to digital, processes the digital signals including spectral analysis, and packetizes the data for transmission. The LPW includes flexible operating configurations that allow for optimizing the scientific return in Mars' ionosphere.

Acknowledgements The authors are grateful to the large number of people who have contributed to the success of this project. In particular we want to acknowledge all the engineers working on the LPW instrument for their creativity and professionalism. The work was made under NASA MAVEN contract (NNH10CC04C).

References

- J.E. Allen, Probe theory—the orbital motion approach. *Phys. Scr.* **45**, 497 (1992). doi:[10.1088/0031-8949/45/5/013](https://doi.org/10.1088/0031-8949/45/5/013)
- S.D. Bale et al., The electric antennas for the STEREO/WAVES experiment. *Space Sci. Rev.* **136**(1–4), 529–547 (2008). doi:[10.1007/s11214-007-9251-x](https://doi.org/10.1007/s11214-007-9251-x)
- J.W. Bonnell, F.S. Mozer, G.T. Delory, A.J. Hull, R.E. Ergun, C.M. Cully, V. Angelopoulos, P.R. Harvey, The Electric Field Instrument (EFI) for THEMIS. *Space Sci. Rev.* **141**(1–4), 303–341 (2008). doi:[10.1007/s11214-008-9469-2](https://doi.org/10.1007/s11214-008-9469-2)
- L.H. Brace, R.F. Theis, A. Dalgarno, The cylindrical electrostatic probes for atmosphere explorer-C, -D, and -E. *Radio Sci.* **8**(4), 341–348 (1973). doi:[10.1029/RS008i004p00341](https://doi.org/10.1029/RS008i004p00341)
- L.B. Brace, Langmuir probe measurements in the ionosphere measurement techniques in space plasmas—particles, in *Geophysical Monograph 102*, ed. by R.F. Pfaff, J.E. Borovsky, D.T. Young (Am. Geophys. Union, Washington, 1998), p. 23
- D.A. Brain, J.S. Halekas, L.M. Peticolas, R.P. Lin, J.G. Luhmann, D.L. Mitchell, G.T. Delory, S.W. Bougher, M.H. Acuña, H. Rème, On the origin of aurorae on Mars. *Geophys. Res. Lett.* **33**, L01201 (1973). doi:[10.1029/2005GL024782](https://doi.org/10.1029/2005GL024782)
- F.F. Chen, Saturation ion currents to Langmuir probes. *J. Appl. Phys.* **36**, 675 (1965). doi:[10.1063/1.1714200](https://doi.org/10.1063/1.1714200)
- J.E.P. Connerney, J. Espley, P. Lawton, S. Murphy, J. Odom, R. Oliverson, D. Sheppard, The MAVEN magnetic field investigation. *Space Sci. Rev.* (2015). doi:[10.1007/s11214-015-0169-4](https://doi.org/10.1007/s11214-015-0169-4)
- C.M. Cully, R.E. Ergun, K. Stevens, A. Nammari, J. Westfall, The THEMIS digital fields board. *Space Sci. Rev.* **141**, 343–355 (2008)
- F. Epavier et al., *Space Sci. Rev.* (2014, this issue)
- R.E. Ergun et al., The FAST satellite field instrument. *Space Sci. Rev.* **98**(1/2), 67–91 (2001)
- R.E. Ergun, L. Andersson, W.K. Peterson, D. Brain, G.T. Delory, D.L. Mitchell, R.P. Lin, A.W. Yau, Role of plasma waves in Mars' atmospheric loss. *Geophys. Res. Lett.* **33**, L14103 (2006). doi:[10.1029/2006GL025785](https://doi.org/10.1029/2006GL025785)

- A.I. Eriksson, R. Boström, R. Gill, L. Åhlén, S.-E. Jansson, J.-E. Wahlund, M. André, A. Mälkki, J.A. Holtet, B. Lybäck RPC-LAP, The Rosetta Langmuir probe instrument. *Space Sci. Rev.* **128**(1–4), 729–744 (2007)
- J.R. Espley, P.A. Cloutier, D.A. Brain, D.H. Crider, M.H. Acuña, Observations of low-frequency magnetic oscillations in the Martian magnetosheath, magnetic pileup region, and tail. *J. Geophys. Res.* **109**, A07213 (2004). doi:[10.1029/2003JA010193](https://doi.org/10.1029/2003JA010193)
- J. Etcheto, H. de Feraudy, J.G. Trotignon, Plasma resonance stimulation in space plasmas. *Adv. Space Res.* **1**(2), 183–196 (1981). doi:[10.1016/0273-1177\(81\)90289-1](https://doi.org/10.1016/0273-1177(81)90289-1)
- U. Fahlson, Theory of electric field measurements conducted in the magnetosphere with electric probes. *Space Sci. Rev.* **7**, 238–262 (1967). doi:[10.1007/BF00215600](https://doi.org/10.1007/BF00215600)
- R. Grard, A. Pedersen, S. Klimov, S. Savin, A. Skalsky, J.G. Trotignon, C. Kennel, First measurements of plasma waves near Mars. *Nature* **341**, 607–609 (1989). doi:[10.1038/341607a0](https://doi.org/10.1038/341607a0)
- D.A. Gurnett, W.S. Kurth, D.L. Kirchner, G.B. Hospodarsky, T.F. Averkamp, P. Zarka, A. Lecacheux, R. Manning, A. Roux, P. Canu et al., The Cassini radio and plasma wave investigation. *Space Sci. Rev.* **114**(1–4), 395–463 (2004)
- D.A. Gurnett, D.L. Kirchner, R.L. Huff, D. Morgan, Radar soundings of the ionosphere of Mars. *Science* **310**, 1929 (2005)
- D.A. Gurnett et al., An overview of radar soundings of the martian ionosphere from the Mars express spacecraft. *Adv. Space Res.* **41**, 1335–1346 (2008)
- J.S. Halekas, E.R. Taylor, G. Dalton, G. Johnson, D.W. Curtis, J.P. McFadden, D.L. Mitchell, R.P. Lin, B.M. Jakosky, The solar wind ion analyzer for MAVEN. *Space Sci. Rev.* (2015). doi:[10.1007/s11214-013-0029-z](https://doi.org/10.1007/s11214-013-0029-z)
- W.B. Hanson, S. Sanatani, D.R. Zuccaro, The Martian ionosphere as observed by the Viking retarding potential analyzers. *J. Geophys. Res.* **82**(28), 4351–4363 (1977). doi:[10.1029/JS082i028p04351](https://doi.org/10.1029/JS082i028p04351)
- P. Harvey, F.S. Mozer, D. Pankow, J. Wygant, N.C. Maynard, H. Singer, W. Sullivan, P.B. Anderson, R. Pfaff, T. Aggson, A. Pedersen, C.-G. Fälthammar, P. Tanskannen, The electric field instrument on the polar satellite. *Space Sci. Rev.* **71**(1–4), 583–596 (1995)
- J.D. Jackson, *Classical Electrodynamics*, 2nd edn. (Wiley, New York, 1975), 92/12/31
- J.P. Krehbiel, L.H. Brace, R.F. Theis, W.H. Pinkus, R.B. Kaplan, The dynamics explorer Langmuir probe instrument. *Space Sci. Instrum.* **5**, 493–502 (1981)
- D.E. Larson et al., *Space Sci. Rev.* (2014, this issue)
- J.-.-P. Lebreton, S. Stverak, P. Travnicek, M. Maksimovic, D. Klinge, S. Merikallio, D. Lagoutte, B. Poirier, P.-L. Blelly, Z. Kozacek, M. Salasquarda, The ISL Langmuir probe experiment processing onboard DEMETER: scientific objectives, description and first results. *Planet. Space Sci.* **54**, 472–486 (2006)
- R. Lundin et al., Solar wind-induced atmospheric erosion at Mars: first results from ASPERA-3 on Mars express. *Science* **305**, 1933–1936 (2004)
- D.M. Malaspina, M. Horanyi, A. Zaslavsky, K. Goetz, L.B. Wilson III, K. Kersten, Interplanetary and interstellar dust observed by the Wind/WAVES electric field instrument. *Geophys. Res. Lett.* **41**, 266–272 (2014). doi:[10.1002/2013GL058786](https://doi.org/10.1002/2013GL058786)
- J.P. McFadden et al., *Space Sci. Rev.* (2014, this issue)
- N. Meyer-Vernet, A. Czechowski, I. Mann, M. Maksimovic, A. Lecacheux, K. Goetz, M.L. Kaiser, O.C. St. Cyr, S.D. Bale, G. Le Chat, Detection of fast nanoparticles in the solar wind. *AIP Conf. Proc.* **1216**, 502 (2010). doi:[10.1063/1.3395912](https://doi.org/10.1063/1.3395912)
- D.L. Mitchell, C. Mazelle, J.A. Sauvaud, D. Toublanc, J.J. Thocaven, J. Rouzaud, A. Federov, E.R. Taylor, M. Robinson, P. Turin, D.W. Curtis, The MAVEN solar wind electron analyzer (SWEA). *Space Sci. Rev.* (2014, this issue)
- H.M. Mott-Smith, I. Langmuir, The theory of collectors in gaseous discharges. *Phys. Rev.* **28**(4), 727–763 (1926). doi:[10.1103/PhysRev.28.727](https://doi.org/10.1103/PhysRev.28.727)
- D. Pankow, R. Besuner, R. Wilkes, R. Ullrich, Deployment mechanisms on the fast satellite: magnetometer, radial wire, and axial booms. *Space Sci. Rev.* **98**(1/2), 93–111 (2001)
- C.M.C. Nairn, R. Grard, A. Skalsky, J.G. Trotignon, Waves and cold plasma observations near Mars. *Adv. Space Res.* **11**(9), 87–91 (1991)
- M.K. Wahlström, E. Johansson, E. Veszelei, P. Bennich, M. Olsson, S. Hogmark, Improved Langmuir probe surface coatings for the Cassini satellite. *Thin Solid Films* **220**(1–2), 315–320 (1992). doi:[10.1016/0040-6090\(92\)90591-X](https://doi.org/10.1016/0040-6090(92)90591-X)
- J.-E. Wahlund, R. Boström Gustafsson, D.A. Gurnett, W.S. Kurth, A. Pedersen, T.F. Averkamp, G.B. Hospodarsky, A.M. Persoon, P. Canu, F.M. Neubauer, M.K. Dougherty, A.I. Eriksson, M.W. Morooka, R. Gill, M. André, L. Eliasson, I. Müller-Wodarg, Cassini measurements of cold plasma in the ionosphere of Titan. *Science* **308**(5724), 986–989 (2005). doi:[10.1126/science.1109807](https://doi.org/10.1126/science.1109807)